Applied Catalysis B: Environmental 258 (2019) 117980

Contents lists available at ScienceDirect

Applied Catalysis B: Environmental

journal homepage: www.elsevier.com/locate/apcatb

A near infrared-activated photocatalyst based on elemental phosphorus by chemical vapor deposition

Qi Zhang[a], Xiangmei Liu[a,*], Lei Tan[a], Zhenduo Cui[b], Xianjin Yang[b], Zhaoyang Li[b], Yanqin Liang[b], Shengli Zhu[b], Kelvin W.K. Yeung[c], Xianbao Wang[a], Yufeng Zheng[d], Shuilin Wu[a,b,*]

[a] Ministry-of-Education Key Laboratory for the Green Preparation and Application of Functional Materials, Hubei Key Laboratory of Polymer Materials, School of Materials Science & Engineering, Hubei University, Wuhan 430062, China
[b] School of Materials Science & Engineering, the Key Laboratory of Advanced Ceramics and Machining Technology by the Ministry of Education of China, Tianjin University, Tianjin 300072, China
[c] Department of Orthopaedics& Traumatology, Li KaShing Faculty of Medicine, The University of Hong Kong, Pokfulam, Hong Kong 999077, China
[d] State Key Laboratory for Turbulence and Complex System and Department of Materials Science and Engineering, College of Engineering, Peking University, Beijing 100871, China

ARTICLE INFO

Keywords:
Phosphorus
Photocatalysis
Near-infrared light
Allotropes
Chemical vapor deposition

ABSTRACT

Phosphorus-based metal-free semiconductors are promising with their non-toxicity and low cost of raw materials. In this work, we synthesized a near-infrared (NIR) activated photocatalyst based on elemental phosphorus (P) by chemical vapor deposition. This photocatalyst consists of black P and another potentially novel red P allotrope which is the major contributor to NIR absorption and photocatalytic activity. The P allotropes of twenty known space groups have been ruled out. The work injects new vitality into the synthesis of P-based photocatalyst and provides a case for synthesis of black P without catalyst at a low pressure. Also, the metal-free photocatalyst with a broad spectral response will be the powerful candidate for further solar-light utility and environmental remediation.

1. Introduction

Since the breakthrough of graphic carbon nitride (g-C_3N_4) as the first metal free photocatalyst in 2010, metal-free photocatalysts has being attracted enhanced attention [1]. Many other simple photocatalysts have been developed, such as elemental photocatalysts (phosphorus, sulfur and boron) with their composites, and even polymers [2–7]. Those photocatalysts based on elemental phosphorus (P) has been studied more widely due to the widespread distribution of P element on the earth. Elemental P, exists in three basic allotropes: white, red, and black. White P is limited to organic chemistry applications due to its low ignition point and high toxicity [8]. The thermodynamically stable but expensive black P had been demonstrated to own semiconductor properties in 2014 and has attracted widespread attention [9–11]. In contrast, red P (RP) is more commonly used because of its low cost, non-toxicity, stability and environmental protection under environmental conditions [12]. RP has been widely used in daily life and industry, such as igniters and chemical analysis [13,14]. Due to the highest theoretical specific capacity among known anode materials for sodium ion batteries [15], RP also has excellent application prospects in the battery field. In 2012, amorphous and Hittorf RP were first discovered to be photocatalytic and used for H_2 evolution [3]. Then RP has been widely studied as a photocatalyst, but its low activity limits its practical application greatly. After that, the small-sized and uniformly distributed fibrous RP showed excellent photocatalytic performance, and the H_2 evolution activity was the highest record in the family of elemental photocatalyst, which greatly stimulated the research on RP [2]. Then in 2017, by introducing fibrous RP in g-C_3N_4, the hybrid exhibited the highest activity of H_2 evolution among all P-containing g-C_3N_4 [4]. Meanwhile, RP as a visible light photocatalyst has great potential in environmental remediation, such as bacterial disinfection, removal of organic pollutants and harmful ions [16,17]. In addition, RP is involved in the synthesis of other P-based photocatalysts, such as NiP [18]. Recently, the research on amorphous RP is also on the rise [19,20]. A series of studies have shown that RP is a hotspot in energy and environmental aspect, especially photocatalytic H_2 evolution. According to the previous researches, the modified RP exhibited slightly different absorption edge from ~680 nm to ~720 nm, corresponding to the colors from bright red (amorphous) to dark red (fibrous type) [12]. However, the known optical absorption property

* Corresponding author.
E-mail addresses: liuxiangmei1978@163.com (X. Liu), shuilin.wu@gmail.com, shuilinwu@tju.edu.cn (S. Wu).

https://doi.org/10.1016/j.apcatb.2019.117980
Received 27 May 2019; Received in revised form 15 July 2019; Accepted 18 July 2019
Available online 20 July 2019
0926-3373/

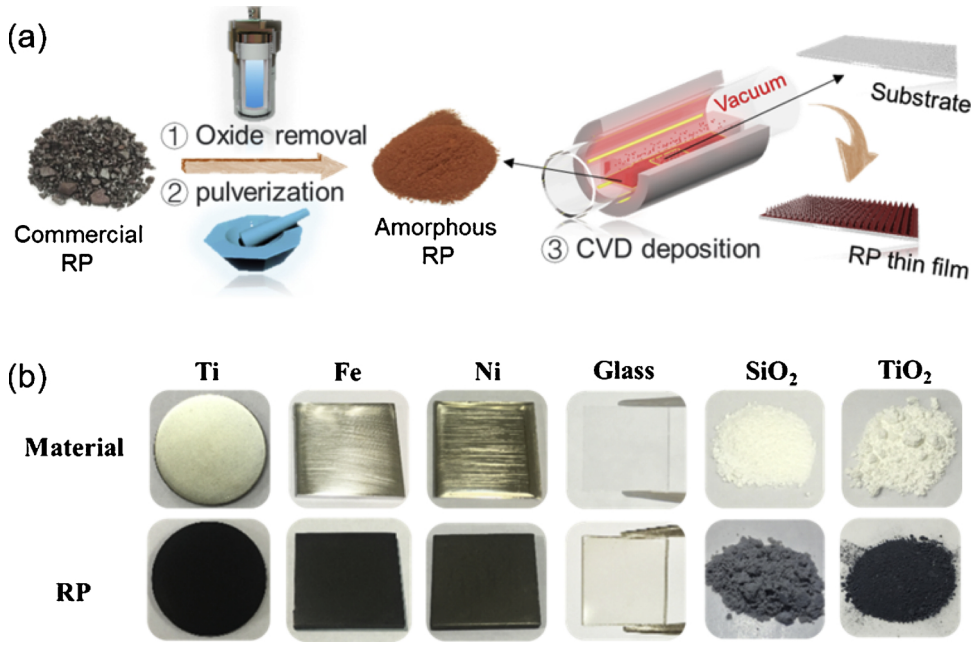

Fig. 1. (a) The synthesis process of the RP film. (b) Optical photograph of various materials before and after deposition of the RP film.

around visible light limits the more efficient utilization of RP to sunlight (visible light only accounts for about 48% of sunlight). Also, the penetration of visible light limit the further application of RP in other fields such as biology. Based on the complex and numerous molecular structures of P allotropes [21,22], we believe that the potential of P as a semiconductor has not been fully realized.

Herein, we present a simple method of chemical vapor deposition (CVD) (Fig. 1a), which could uniformly form a black film on the surface of various materials (Fig. 1b). Furtherly, we have studied the properties of deposited black film in detail using the film grown on the surface of titanium plates (Ti-RP). It is found that Ti-RP not only has strong absorption in NIR (accounts for about 44% of sunlight), but also exhibits good photocatalytic activity (the photocatalytic production of superoxide anion and singlet oxygen).

2. Experimental section

2.1. Preparation of RP film

Firstly, 6.0 g commercial RP is hydrothermally reacted for 12 h at 200 ℃ to removed the oxides on the surface. Then the RP is pulverized and kept in Ar atmosphere for future use. Next, 0.6 g amorphous RP is placed in a porcelain crucible owned a porcelain lid (separate, not one-piece and sealed) together with appropriate substrates (*e.g.* Ti). As for powders (*e.g.* TiO_2), it is mixed with the amorphous RP uniformly in advance. A vacuum is maintained before temperature elevation. The high temperature of 750 ℃ is maintained for 1 h and then 280 ℃ is maintained for 12 h. After the device gradually decreasing to environment temperature, the black RP film is obtained.

2.2. Characterization

Scanning Electron Microscope (SEM) images are obtained from Field-emission SEM (Zeiss sigma 500, Germany). The transmission electron microscopy (TEM) and high-resolution TEM images are acquired on ZEISS Libra 200 FE TEM. Raman spectra are recorded by a confocal Raman microspectroscope (Renishaw, UK). X-ray diffraction (XRD) patterns are obtained by an X-ray diffraction spectrometer (D8A25, Bruker, Germany) with the metal target is Cu (λ = 1.540598 Å) and a step size of 0.02°. X-ray photoelectron spectra (XPS) are acquired on an ESCALAB 250Xi instrument (Thermo Fisher Scientific, USA). The UV–vis-NIR absorption spectra are transformed from the diffuse reflectance spectra (DRS), which are investigated by a UV–vis-NIR spectrophometer (UV–vis-NIR, UV-3600, Shimadu, Japan) with an integrating sphere attachment which $BaSO_4$ is as reflectance standard. The ultraviolet photoelectron spectroscopy (UPS) is measured on an ESCALAB 250Xi instrument with a monochromatic He I light source (21.22 eV). The ESR measurement irradiated for 60 min under ice water bath is performed by JES-FA200 spectrometer (JEOL, Tokyo, Japan) at room temperature.

2.3. Photoelectrochemical (PEC) measurement

A three-electrode system, equipped with a Pt electrode as counter electrode and Ag/AgCl electrode as a reference electrode, is used in all the PEC experiments with 0.5 M Na_2SO_4 aqueous solution as electrolyte. The samples are served as working electrode using an electrochemical analyzer (CHI-660E, Shanghai Chenhua) with a light source (808 nm, LOS-BLD-0808). The scan rate of LSV is 10 mV/s. The Mott-Schotty plot is conducted under a frequency of 1000 Hz.

2.4. Photocatalytic experiments

All the measurements are conducted under ice water bath to minimize the influence of temperature under irradiation. A 808 nm light (LOS-BLD-0808) is served as light source. All the absorption spectra are measured on a microplate reader (SpectraMax I3MD USA).

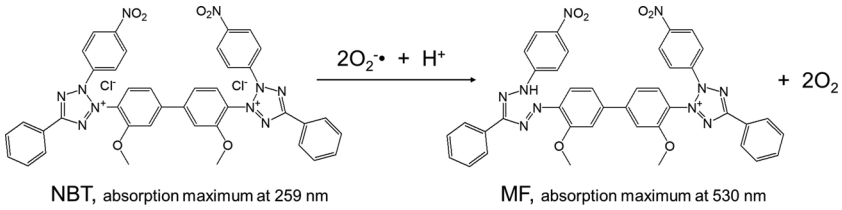

2.4.1. NBT (nitro blue tetrazolium) method for detection of O_2^-•

NBT dimethyl sulfoxide (DMSO) solution (2.5×10^{-5} mol/L) is used with 808 nm light (0.45 W/cm^2). The amount of O_2-• is indirectly obtained by detecting the absorption spectra of generated MF. Before illumination, all groups are oscillated for 15 min to mix evenly. After illumination, the solution is oscillated for 5 min to mix evenly, and then 300 u l solution is taken to test the absorption spectra.

2.4.2. Detection of $^1O_2$ by 1, 3-Diphenylisobenzofuran (DPBF)

DPBF DMSO solution (10 μg/mL) is employed with 808 nm light (0.45 W/cm^2). The DPBF is acted as the trapping agent of $^1O_2$. Before illumination, all groups are oscillated for 10 min to mix evenly. After illumination, the solution is oscillated for 3 min to mix evenly, and then 300 μl solution is taken to test the absorption spectra.

3. Results and discussion

In a typical synthesis, the amorphous RP (Fig. S1) is used as starting material, which is obtained from commercial RP by hydrothermal reaction at 200 °C for 12 h to remove oxides and pulverization to acquire fine powders. It is placed in a porcelain crucible owned lid together with appropriate substrates (*e.g.* Ti). As for powders (*e.g.* TiO_2), it is mixed with the amorphous RP uniformly in advance. A vacuum is maintained before temperature elevation. After the device gradually decreases to environment temperature, black films are obtained on various materials. Since the film is converted from amorphous RP, it is named RP film. In the following process, we explore the RP film deposited on the surface of Ti in detail.

Fig. 2a shows that a film of substantially uniform density and spatial distribution is grown on Ti. The inset image reveals that the structure unit shows irregularly pyramidal shape. Besides, the cross-sectional view exhibits that the film is composed of a plurality of pyramids and the film thickness is about 0.89 μm (Fig. 2b). Based on the above morphology, we consider the film as an array of irregular pyramids. Besides, the higher aspect ratio surface structure along with the higher roughness may be beneficial to the light absorption [23]. In order to further study the microstructure of the film, the film from the substrate were removed by rubbing with a blade for the TEM study. The Fig. 2c shows that the morphology unit contains many small nanoparticles even quantum dots. To identify these whether structures are not unique, another larger nanosheet (Fig. S2) shows wide and homogeneous distribution of nanoparticles. Due to the TEM sample was dispersed by ultrasound in preparation, the fine particles around the large size sample may be the ultrasonically detached nanoparticles, according to their similar size. Besides, the HRTEM image (Fig. 2d) displays clear lattice fringes with d-spacing of 0.52 nm and 0.264 nm, corresponding to the (002) and (004) plane for BP (identified from PDF#09-0020), while it also shows a d-spacing of 0.218 nm for another component. In this way, the RP film on Ti is more likely to be a mixture, in which BP is one of the components. Furthermore, since the components in the RP film are formed at the same time under the same condition, it is unlikely for the components to own an obvious distribution range and boundary, like the semiconductor composites with a sequential synthesis process. Instead, they are more likely to be randomly and evenly distributed, which is appeared on the HRTEM image.

In order to further study the chemical structure of the RP film, XPS, Raman spectra and XRD of the Ti-RP are performed. As shown in Fig. 3a, both P 2p and P 2 s peaks can be identified from the survey spectrum, indicating the growth of RP film on the surface of Ti [24].

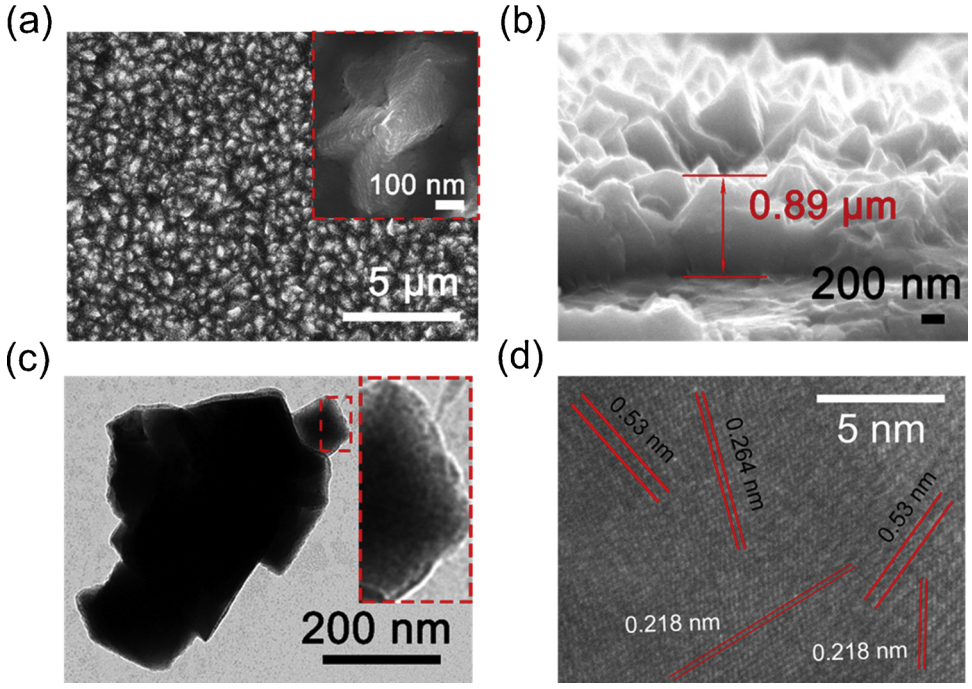

Fig. 2. (a) SEM image and (b) cross-view image of Ti-RP. (c) TEM and (d) high-resolution TEM image of the RP film.

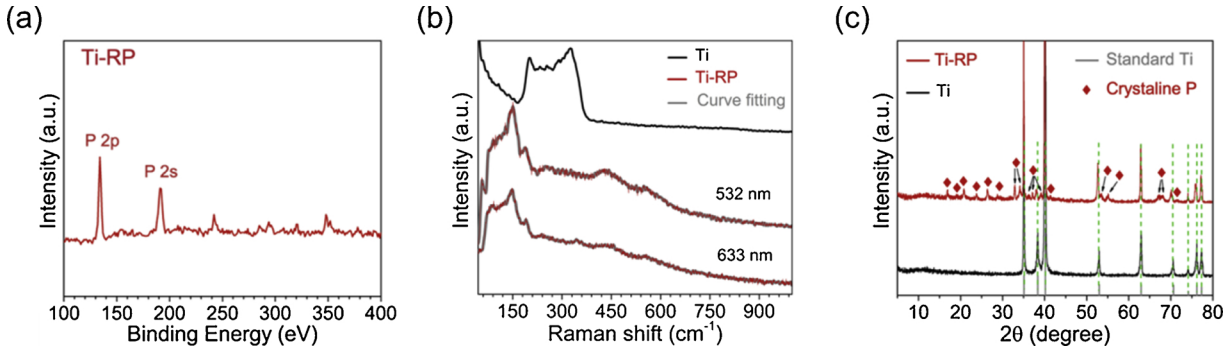

Fig. 3. (a) XPS survey spectra of Ti-RP. (b) Raman spectra of Ti and Ti-RP at the excitation light of 532 nm and 633 nm. The gray lines represent the smooth fitting performed using the Savitzky-Golay algorithm at the level of 1%. (c) XRD of Ti and Ti-RP. The peaks of standard Ti is obtained from PDF standard card (65–9622). The red squares are the crystalline peaks of the RP film. (For interpretation of the references to colour in this figure legend, the reader is referred to the web version of this article).

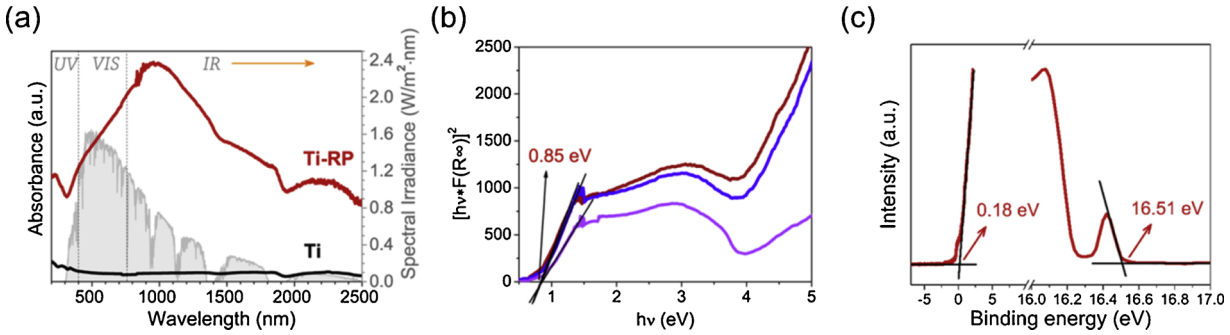

Fig. 4. (a) The UV–vis-NIR diffuse reflectance spectra (DRS) of Ti and Ti-RP. The inset gray background is the solar irradiation spectrum. (b) The corresponding tauc plots derived from DRS which the RP film is regarded as a direct bandgap semiconductor. (c) UPS measurement of Ti-RP with a monochromatic He I light source (21.22 eV).

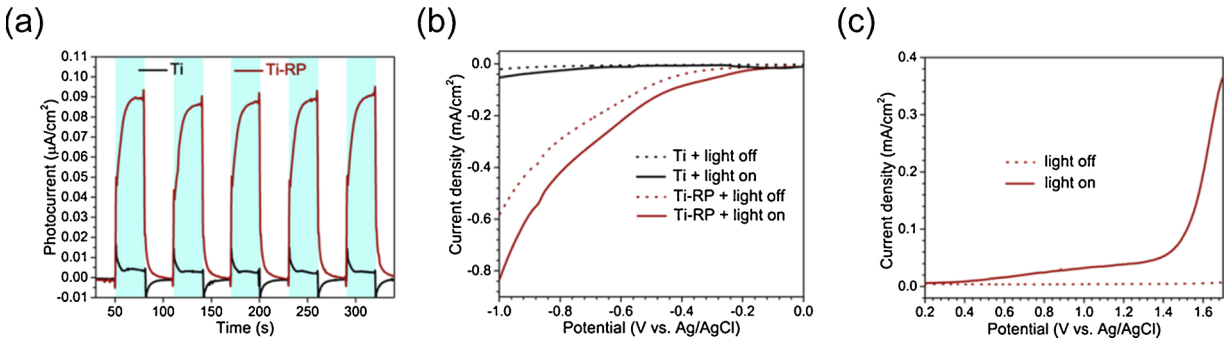

Fig. 5. (a) Photocurrent responses of Ti-RP under a 808 nm light. (b) Negative sweep and (c) positive sweep of linear sweep voltammetry (LSV) of Ti and Ti-RP. The irradiation is provided by a 808 nm laser. The optical density (OD) remained constant during the tests.

Raman spectra are acquired on the samples of Ti and Ti-RP at the excitation of 532 nm (Fig. 3b). The Raman spectrum of Ti-RP at the excitation of 633 nm is also exhibited. Because the original lineshape noise is relatively large, to be more intuitive, we utilize the Savitzky-Golay algorithm to perform a smooth fitting at the level of 1%, which is shown by the gray curve. The Raman spectra along with the curves fitted to individual peaks are shown in Fig. S3a and S3b. It can be seen that whether the excitation light is 532 nm or 633 nm, the lineshape can be perfectly fitted to the 8 peaks, and the positions are very similar. A few differences would be due to the necessary smoothing and baseline subtraction process in the fitting. The similarity of the Raman spectra with the two excitation lights with different penetration depths indicates the uniformity of the film. Besides, the lineshapes of Ti-RP are completely changed with respect to Ti, indicating that Ti has been covered by a dense RP film. They also show that intensity exists over the region of 50-700 cm^{-1}, and no pronounced gap is observed. The primary Raman signals appear at 50-200 cm^{-1}, whereas less-intense bands appear at 210-700 cm^{-1}. The Raman peaks in the frequency range up to 140 cm^{-1} correspond to vibrations of the structural cluster against each other (very large mass) and the weak restoring forces (van der Waals forces provide some of the bonding between the clusters), which are expected at low frequency [25]. The strong peaks at the low frequency in Ti-RP indicate that the presence of structural clusters and the high long range order correlation between the clusters, and further reveal the existence of crystalline state of the RP film [25]. Bands around 200 cm^{-1} may be contributed by the vibrations related to bond angle distortions, while frequencies above 340 cm^{-1} would be the vibrations of bond bending and bond stretching nature in cluster [25–28]. According to previous reports [2,29,30], the main peaks of the Raman spectra of various P allotropes are known in Fig. S3c. Although the whole lineshape and the relative intensity of Ti-RP are very different from the one of the P allotropes, in order to be more scientific, the

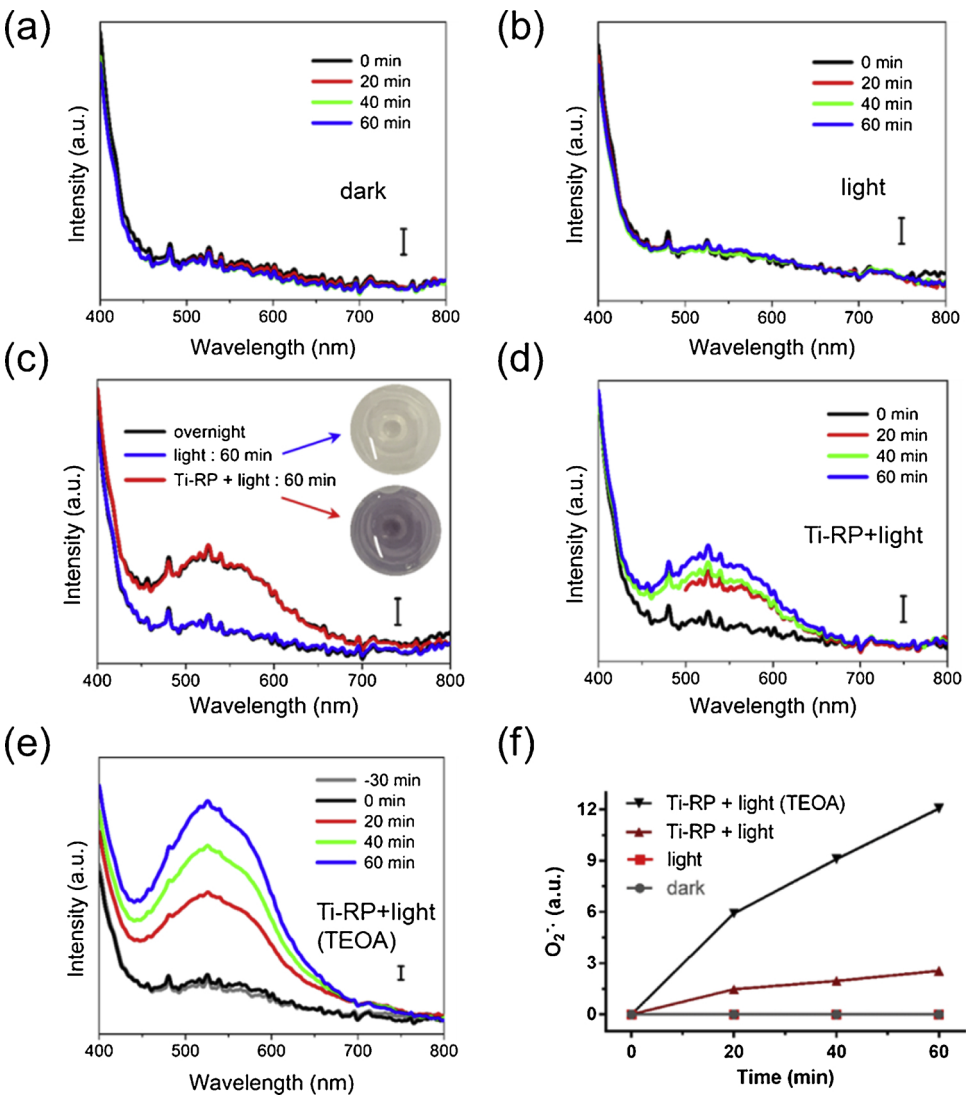

Fig. 6. Superoxide anion characterization. Photocatalytic production of $O_2^{-}\cdot$ by Ti-RP detected by NBT method (light :808 nm, 0.45 W/cm^2). The absorption spectra of MF in groups of (a) dark without Ti-RP, (b) irradiation without Ti-RP. And the absorption spectra in (c) the light group and the Ti-RP + light group that have been irradiated for 60 min and left overnight, (d) the group of irradiation with Ti-RP, as well as (e) the group of irradiation with Ti-RP and additional 1% (v/v) of triethanolamine (TEOA) as hole scavenger. The scale bar in the figures represent the OD value of 0.01. Oscillation for 5 min after each illumination to mix well, and 300 μL of liquid is sucked out for measurement. (f) The quantification of the above spectra.

possibility of the presence of the allotropes cannot be simply ruled out due to the broad band of 300-500 cm^{-1}. According to Fasol et al. [26] and Olego et al. [27], we judge the absence of pentagonal cages and further the absence of Hittorf and fibrous P in our sample (Section S1).

XRD is used to further analyze the structure of RP film (Fig. 3c). According to the peaks, it can be confirmed that the synthesized RP film is crystallized, which is consistent with the results of HRTEM and Raman spectra before. After excluding the peaks of Ti, the crystallized P can be identified at least 17 peaks (marked with red squares). In this work, if all the major strong peaks of a P allotrope can correspond to the positions of the crystallized P one-to-one, it can be speculated that this P allotrope exists in RP film. The standard XRD patterns of various P allotropes for comparison are given in Fig. S4-S7. From the detailed comparison in Section S2, it can be confirmed that the RP film has black P (Bmab) and does not belong to any RP allotropes of type I–V. Also, other P allotropes of the 15 different space groups mentioned are also excluded out of our sample. Base on the XRD analysis and the different Raman spectra (intensity persists over a broad range, strong peaks exist in the low frequency region), we boldly guess that at least 8 other unknown peaks after excluding the peaks of black P are likely to belong a new RP allotrope (due to the transition from amorphous RP).

In order to provide more evidences, we test the optical properties of the samples and find a very strong absorption in NIR region. The absorption lineshape is very different from that of black P, but somewhat similar to $Cu_2(OH)PO_4$ (Fig. 4a) [31]. The absorption observed beyond 2000 nm would be attributed to the lattice stretching modes [31]. In addition, the NIR absorption of Ti-RP can fitted into with three Gaussian peaks centered at 412, 980 and 1800 nm (at 3.01, 1.26 and 0.69 eV, respectively; Fig. S8a). And the absorption is strongest in NIR centered at 980 nm. However, regardless of bulk BP or BP quantum dots, the high absorbance is mainly concentrated in visible light region [32–34]. To be more scientific, the diffuse reflectance spectra of Ti-RP, which were obtained from three measurements, are also provided (Fig. S8b). The same absorption trend can be observed, which reveals the absorption intensity of Ti-RP in visible range increases along with the wavelength, rather than decreases like black P. The significant difference from the black P indicates that the absorption in NIR region is mainly attributed to the RP allotrope rather than black P. In order to support this conclusion more strongly, we deposited the RP film on the surface of anatase TiO_2 powder as the same process. The corresponding XRD is very similar with Ti-RP without the typical peaks of black P (Fig. S9a). The corresponding absorption spectrum reveals that in addition to the absorption of typical anatase TiO_2, there is significant absorption in NIR region (Fig. S9b), which should be attributed to the RP allotrope instead of the impurity level in TiO_2 [35,36]. Moreover, the differences of XRD (Fig. S10), DRS, and photocatalytic activity (that of Ti-RP is studied below) between the RP film and TiP, has ruled out the presence of the composition directly formed by Ti and P, *i.e.*, TiP [37,38]. In summary, we synthesize a RP film strongly absorbed in NIR region, and the composition is very likely of a mixture of black P and another RP

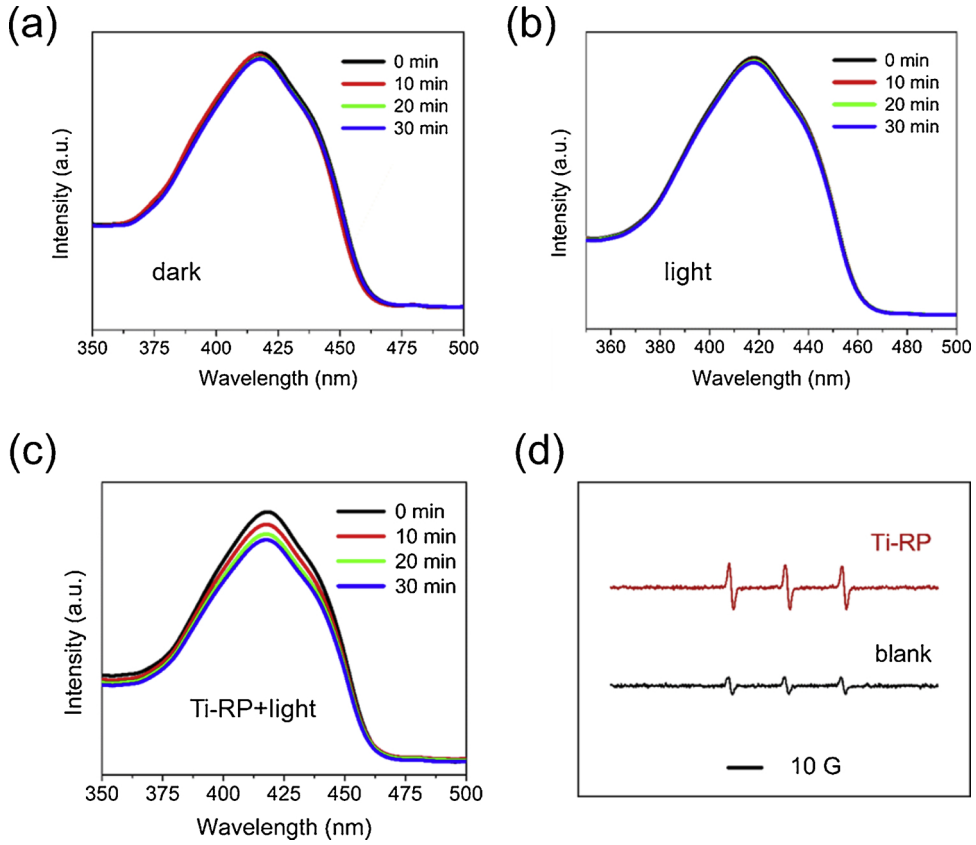

Fig. 7. Singlet oxygen characterization. Time dependent absorption spectra of the DPBF in groups of a) dark without Ti-RP, b) irradiation without Ti-RP. (c) irradiation with Ti-RP. (light :808 nm, 0.45 W/cm^2) (d) ESR spectra in the presence of TEMP for $^1O_2$ detection.

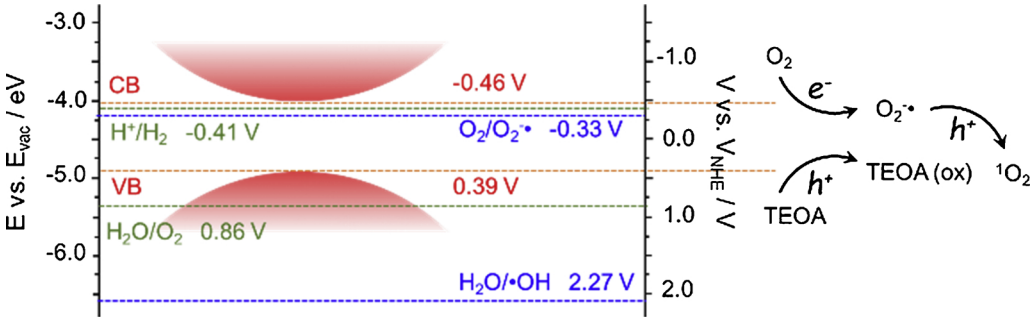

Fig. 8. The band structure of the synthesized film.

allotrope. The growth mechanism of black P on the surface of Ti, the specific atomic structure of the RP allotrope, and the respective purification methods will be further investigated in the future.

To obtain the bandgap of the RP film, Tauc plots are converted from the UV–vis-NIR diffuse reflectance spectra (DRS; Fig. 4b and Fig. S11). The calculated bandgap of the RP film would be identified as about 0.85 eV (Section 3), which is close to that of 2–3 layers of black P [39]. In order to further explore the band structure of the RP film, ultraviolet photoelectron spectroscopy (UPS) is employed to estimate the valence-band maximum (VB) (Fig. 4c). According to Han et al. [40], the calculated work function (Φ) is 4.71 eV (Φ = 21.22 eV – 16.51 eV), while the energy difference between VB and Φ is 0.18 eV. In this way, the VB is about -4.89 eV *vs.* vacuum. As such, the VB and conduction-band minimum (CB) are about 0.39 and -0.46 V (*vs.* NHE), respectively. The CB provides a sufficient overpotential for the production of superoxide anion ($O_2^{-}\bullet$) [41]. To investigate whether the RP film responses to photo energy of NIR, the photoelectrochemical tests are conducted. As a typical NIR monochromatic light (IR: λ > 760 nm) [42,43], 808 nm light is selected as the light source due to its representativeness in NIR and wide use in various biological applications. Under non-bias and sacrificial agents, Ti-RP exhibits a significantly increased transient photocurrent compared to Ti, indicating that the RP film can effectively generate free photogenerated charge carriers under irradiation, which provides possibility for photocatalytic reactions (Fig. 5a). Fig. 5b and c are the negative sweep and positive sweep of linear sweep voltammetry (LSV) curves, respectively. Compared to the one in the dark, there is a significant increase in photocurrent under irradiation, while Ti has little difference, indicating the effective separation of electron-hole pairs in RP film. In a word, photoelectrochemical measurements show that RP film can produce photogenerated electrons under NIR irradiation for the potential of photocatalysis.

To verify that Ti-RP does have photocatalytic activity under NIR irradiation, Nitro Blue Tetrazolium (NBT) method is used to specially detect $O_2^{-}\bullet$ [44], which NBT can react with $O_2^{-}\bullet$ to produce monoformazan (MF) that exhibits a maximum absorbance at 530 nm [45]. Hence, comparing the absorbance of MF, we could evaluate the

concentration of O_2^{-}•. As shown in Fig. 6a and b, NTB solution does not generate MF by itself, and light has no effect on MF production. Even after the group of light and the group of Ti-RP + light that have been irradiated for 60 min were left overnight, the absorption spectra have no change, which reveals that no MF is generated (Fig. 6c). The above results demonstrate that light or Ti-RP alone has no effect on the formation of MF. However, when the NBT solution containing Ti-RP was illuminated, MF production showed an increasing trend with time (Fig. 6d). The optical images of solution in groups of light and Ti-RP + light after 60 min irradiation further confirm the generation of MF (Fig. S12) Besides, the rate of MF production is significantly increased when 1% TEOA (v/v) that reacts more easily with holes to inhibit electron-hole pairs recombination is added (Fig. 6e). To be more intuitive, the absorption spectra of these groups are correspondingly quantified as shown in Fig. 6f. The results indicates that O_2^{-}• is formed from Ti-RP with irradiation, and is closely related with the photogenerated electrons. Therefore, we conclude that the RP film has photocatalytic activity under NIR and its conduction band position is higher than or equivalent to the potential for redox couple O_2/ O_2^{-}• (-0.33 V *vs.*NHE, pH = 7). It is consistent with the previous conclusion of UPS and the calculated bandgap. Also, the electrochemical flat-band potential is gained from the Mott-Schotty plot is about -0.9 V *vs.* Ag/AgCl, *i.e.*, -0.7 V *vs.* NHE (electrolyte : 0.5 M Na_2SO_4, pH = 6), which is also higher than the potential for redox couple O_2/ O_2^{-}• and revealed that the RP film can produce O_2^{-}• (Fig. S13) [41].

To investigate whether the RP film can produce other reactive oxygen species (ROS), the photodegradation of 1, 3-diphenylisobenzofuran (DPBF) and electron spin resonance (ESR) spectrum are conducted to detect singlet oxygen ($^1O_2$). The decline of absorption peak around 415 nm represents the generation of $^1O_2$, which DPBF reacts with $^1O_2$ through Diels–Alder 1, 4-cycloaddition [46]. As shown in Fig. 7a and b, the groups of dark and light both show negligible decrease of DPBF, while the group of Ti-RP + light show significant decline (Fig. 7c). The result illustrates the photodegradation of DPBF, which further reveals the generation of $^1O_2$ by Ti-RP. Besides, ESR, the most common evidence for identifying $^1O_2$, is also provided. Trapping agent is 2,2,6,6-tetramethylpiperidine (TEMP). As shown in Fig. 7d, the relative intensities of the signals in the group of Ti-RP after irradiation are greatly enhanced, which also indicates the production of $^1O_2$ [47,48]. Based on above tests, we conclude that the RP film own photocatalytic activity at 808 nm, *i.e.*, in NIR.

The generation of O_2^{-}• and $^1O_2$ has been confirmed above. According to Nosaka et al., the generation of $^1O_2$ is associated not only with electrons but also with holes (O_2 + e- → O_2^{-}•, O_2^{-}• + h^+ → $^1O_2$) [49]. Besides, both nanosheet and bulk BP can produce $^1O_2$ efficiently, which indicates the bandgap has little effect on whether $^1O_2$ can be produced (the bandgap of BP varies with the number of layers) [46]. The BP in RP films may partly contribute to the formation of $^1O_2$, but the production of O_2^{-}• must be entirely owed to the potentially new RP allotrope, which the detectable ROS generated by pure BP in NIR can only be $^1O_2$ [46,48]. This also indirectly verified the existence of a novel RP allotrope with NIR photocatalytic properties, which supports the previous guess. Combined with the potentials for various redox couple, a band structure of the RP film is given in Fig. 8. And it can be seen that the RP film not only can generate ROS under NIR, but also would have potential in hydrogen production. To investigate if the photocatalytic activity is limited to Ti-RP, the test about NBT method is also conducted on Fe-RP as a instance. As shown in Fig. S14, the peak at 530 nm reveals the generation of MF, which further indicates the production of O_2^{-}•, that is, the RP film on Fe also owns photocatalytic activity. The result illustrates the possibility of photocatalytic activity on other substrates. Also, the morphology of the RP film on Fe is also investigated (Fig. S15). Although many protuberances are shown on the film, large difference is with the RP film on Ti. We speculate that not only does the smoothness of the substrate affect the structure of the RP film, but the substrate itself does.

4. Conclusion

In summary, we demonstrate a simple method which can deposit a black film uniformly on the surface of various materials. The film on Ti is in the morphology of an irregular pyramid array, which has strong absorption and photocatalytic activity in the NIR. Besides, the film consists of black phosphorus (Bmab) and another potentially novel P allotrope, which is major contributor to NIR absorption and photocatalytic activity. This work not only provides a way for metal-free NIR photocatalysts, but also a case for low-pressure catalyst-free synthesis of black P. Moreover, the higher conduction band position endows the photocatalyst the capacity for ROS generation and the possibility in hydrogen production, which supply an option for more efficient solar-energy utility in fields of environmental remediation and energy regeneration.

Declaration of Competing Interest

The authors declare that they have no known competing financial interests or personal relationships that could have appeared to influence the work reported in this paper.

Acknowledgements

This work is jointly supported by the National Natural Science Foundation of China, Nos. 51671081, 51871162, 51801056 and 51422102, and the National Key R&D Program of China No. 2016YFC1100600 (sub-project 2016YFC1100604), and Natural Science Fund of Hubei Province, 2018CFA064.

Appendix A. Supplementary data

Supplementary material related to this article can be found, in the online version, at doi:https://doi.org/10.1016/j.apcatb.2019.117980.

References

[1] X. Wang, K. Maeda, A. Thomas, K. Takanabe, G. Xin, J.M. Carlsson, K. Domen, M. Antonietti, Nat. Mater. 8 (2008) 76.
[2] Z. Hu, L. Yuan, Z. Liu, Z. Shen, J.C. Yu, Angew. Chem. Int. Ed. 55 (2016) 9580–9585.
[3] F. Wang, W.K.H. Ng, J.C. Yu, H. Zhu, C. Li, L. Zhang, Z. Liu, Q. Li, Appl. Catal. B: Environ. 111 (2012) 409–414.
[4] L. Jing, R. Zhu, D.L. Phillips, J.C. Yu, Adv. Funct. Mater. 27 (2017) 1703484.
[5] G. Liu, L.C. Yin, P. Niu, W. Jiao, H.M. Cheng, Angew. Chem. Int. Ed. 52 (2013) 6242–6245.
[6] A.S. Weingarten, R.V. Kazantsev, L.C. Palmer, M. McClendon, A.R. Koltonow, A.P.S. Samuel, D.J. Kiebala, M.R. Wasielewski, S.I. Stupp, Nat. Chem. 6 (2014) 964.
[7] G. Liu, P. Niu, L. Yin, H.M. Cheng, J. Am. Chem. Soc. 134 (2012) 9070–9073.
[8] S. Carenco, I. Resa, X. Le Goff, P. Le Floch, N. Mézailles, Chem. Commun. 22 (2008) 2568–2570.
[9] R. Gusmão, Z. Sofer, M. Pumera, Angew. Chem. Int. Ed. 56 (2017) 8052–8072.
[10] W. Lei, G. Liu, J. Zhang, M. Liu, Chem. Soc. Rev. 46 (2017) 3492–3509.
[11] L. Li, Y. Yu, G.J. Ye, Q. Ge, X. Ou, H. Wu, D. Feng, X.H. Chen, Y. Zhang, Nat. Nanotechnol. 9 (2014) 372.
[12] Z. Hu, Z. Shen, J.C. Yu, Green Chem. 19 (2017) 588–613.
[13] E.C. Koch, Propellants, Explos., Pyrotech. 33 (2008) 165–176.
[14] M. Scheer, G. Balázs, A. Seitz, Chem. Rev. 110 (2010) 4236–4256.
[15] S. Liu, J. Feng, X. Bian, J. Liu, H. Xu, Y. An, Energy Environ. Sci. 10 (2017) 1222–1233.
[16] W. Wang, G. Li, T. An, D.K. Chan, J.C. Yu, P.K. Wong, Appl. Catal. B: Environ. 238 (2018) 126–135.
[17] D. Xia, Z. Shen, G. Huang, W. Wang, J.C. Yu, P.K. Wong, Environ. Sci. Technol. 49 (2015) 6264–6273.
[18] W. Wang, T. An, G. Li, D. Xia, H. Zhao, J.C. Yu, P.K. Wong, Appl. Catal. B: Environ. 217 (2017) 570–580.
[19] S. Zhang, H. Qian, Z. Liu, H. Ju, Z. Lu, H. Zhang, L. Chi, S. Cui, Angew. Chem. Int. Ed. 58 (2019) 1659–1663.
[20] P.E.M. Amaral, G.P. Nieman, G.R. Schwenk, H. Jing, R. Zhang, E.B. Cerkez, D. Strongin, H.F. Ji, Angew. Chem. Int. Ed. 58 (2019) 6766–6771.
[21] M. Haeser, J. Am. Chem. Soc. 116 (1994) 6925–6926.
[22] H.G. von Schnering, Angew. Chem. Int. Ed. 20 (1981) 33–51.
[23] X. Wang, Q. Liu, S. Wu, B. Xu, H. Xu, Adv. Mater. 31 (2019) 1807716.
[24] X. Bai, Y. Du, X. Hu, Y. He, C. He, E. Liu, J. Fan, Appl. Catal. B: Environ. 239 (2018)

204–213.
[25] D.J. Olego, J.A. Baumann, M.A. Kuck, R. Schachter, C.G. Michel, P.M. Raccah, Solid State Commun. 52 (1984) 311–314.
[26] G. Fasol, M. Cardona, W. Hönle, H.G. von Schnering, Solid State Commun. 52 (1984) 307–310.
[27] D.J. Olego, J.A. Baumann, R. Schachter, Solid State Commun. 53 (1985) 905–908.
[28] C. Grotz, K. Schäfer, M. Baumgartner, R. Weihrich, T. Nilges, Inorg. Chem. 54 (2015) 10794–10800.
[29] R.A.L. Winchester, M. Whitby, M.S.P. Shaffer, Angew. Chem. Int. Ed. 48 (2009) 3616–3621.
[30] J.B. Smith, D. Hagaman, D. DiGuiseppi, R. Schweitzer-Stenner, H.-F. Ji, Angew. Chem. Int. Ed. 55 (2016) 11829–11833.
[31] G. Wang, B. Huang, X. Ma, Z. Wang, X. Qin, X. Zhang, Y. Dai, M.-H. Whangbo, Angew. Chem. Int. Ed. 52 (2013) 4810–4813.
[32] X.F. Jiang, Z. Zeng, S. Li, Z. Guo, H. Zhang, F. Huang, Q.H. Xu, Materials 10 (2017) 210.
[33] X. Zhang, H. Xie, Z. Liu, C. Tan, Z. Luo, H. Li, J. Lin, L. Sun, W. Chen, Z. Xu, L. Xie, W. Huang, H. Zhang, Angew. Chem. Int. Ed. 54 (2015) 3653–3657.
[34] C. Mao, Y. Xiang, X. Liu, Z. Cui, X. Yang, Z. Li, S. Zhu, Y. Zheng, K.W.K. Yeung, S. Wu, ACS Nano 12 (2018) 1747–1759.
[35] J. Chen, Z. Liu, Y. Wu, Y. Li, J. Zhao, X. Zhu, P. Na, Chem. Commun. 54 (2018) 1972–1975.
[36] K. Wang, J. Yu, L. Liu, L. Hou, F. Jin, Ceram. Int. 42 (2016) 16405–16411.
[37] M. Knausenberger, G. Brauer, K.A. Gingerich, J. Less-Common Met. 8 (1965) 136–148.
[38] C. Blackman, C.J. Carmalt, I.P. Parkin, S. O'Neill, L. Apostolico, K.C. Molloy, S. Rushworth, Chem. Mater. 14 (2002) 3167–3173.
[39] G. Zhang, S. Huang, A. Chaves, C. Song, V.O. Özçelik, T. Low, H. Yan, Nat. Commun. 8 (2017) 14071.
[40] W. Chen, Y. Wu, Y. Yue, J. Liu, W. Zhang, X. Yang, H. Chen, E. Bi, I. Ashraful, M. Grätzel, L. Han, Science 350 (2015) 944–948.
[41] J. Kou, C. Lu, J. Wang, Y. Chen, Z. Xu, R.S. Varma, Chem. Rev. 117 (2017) 1445–1514.
[42] J. Wang, Y. Li, L. Deng, N. Wei, Y. Weng, S. Dong, D. Qi, J. Qiu, X. Chen, T. Wu, Adv. Mater. 29 (2017) 1603730.
[43] W. Wang, Y. Li, Z. Kang, F. Wang, J.C. Yu, Appl. Catal. B: Environ. 182 (2016) 184–192.
[44] H.Y. Jiang, P. Zhou, Y. Wang, R. Duan, C. Chen, W. Song, J. Zhao, Adv. Mater. 28 (2016) 9776–9781.
[45] R. Liu, S. Fu, H. Zhan, L.A. Lucia, Ind. Eng. Chem. Res. 48 (2009) 9331–9334.
[46] H. Wang, X. Yang, W. Shao, S. Chen, J. Xie, X. Zhang, J. Wang, Y. Xie, J. Am. Chem. Soc. 137 (2015) 11376–11382.
[47] G. Li, C. Guo, M. Yan, S. Liu, Appl. Catal. B: Environ. 183 (2016) 142–148.
[48] H. Wang, S. Jiang, W. Shao, X. Zhang, S. Chen, X. Sun, Q. Zhang, Y. Luo, Y. Xie, J. Am. Chem. Soc. 140 (2018) 3474–3480.
[49] Y. Nosaka, A.Y. Nosaka, Chem. Rev. 117 (2017) 11302–11336.